GDCh Research Article Angewandte International Edition Chemie www.angewandte.org

How to cite: *Angew. Chem. Int. Ed.* **2026**, *65*, e24999
doi.org/10.1002/anie.202524999

High-Pressure Chemistry

Experimental Observation of a Calcium Silicon Double Carbonate

Benedito Donizeti Botan-Neto, David Santamaria-Perez,* Julia Bungarten, Lkhamsuren Bayarjargal, Björn Winkler, Alberto Otero-de-la-Roza, and Bihan Wang*

Abstract: Reactions between carbon dioxide (CO_2) and silica (SiO_2), as well as between carbonates and silicates, are central to understanding carbon behavior in planetary interiors and have important technological implications. Yet, only a few oxides are known in which carbon and silicon coexist within the same crystal lattice. These silicate–carbonates typically contain trigonal carbonate [CO_3] groups and tetrahedrally coordinated silicate [SiO_4] units. In the CaO–SiO_2–CO_2 system, no phase had previously been shown to contain both octahedrally coordinated silicon [SiO_6] and carbonate [CO_3] groups, nor had such a structure been theoretically predicted. Here, we report the synthesis of the calcium silicon double carbonate $Ca_2Si(CO_3)_4$, obtained by reacting tilleyite, $Ca_5(Si_2O_7)(CO_3)_2$, with CO_2 in diamond anvil cells at 39.5 GPa and 2600 K. The compound was subsequently temperature- and pressure-quenched, remaining metastable at ambient conditions. Structural and spectroscopic characterization was performed using synchrotron single-crystal X-ray diffraction and Raman spectroscopy. The structure of $Ca_2Si(CO_3)_4$ is unique among silicate–carbonates, featuring sixfold-coordinated Si sharing oxygen atoms with [CO_3] groups. Additionally, a novel calcium tetracarbonate, $Ca_2(C_4O_{10})$, containing tetrahedral [CO_4] units, was discovered. These findings reveal a new oxide chemistry under extreme conditions and open avenues for synthesizing metastable carbon-bearing materials relevant to the deep carbon cycle.

Introduction

Carbon dioxide (CO_2) is both highly abundant and of fundamental importance in the Universe. It plays a key role in planetary atmospheres, where it is a major constituent of Earth-like planets, and is also present in solid icy phases on outer planets and asteroids.[1,2] Under ambient conditions, CO_2 exists as a gas, and its increasing concentration in Earth's atmosphere poses a significant challenge to human societies and ecosystems.[3] Upon compression, carbon dioxide first forms a series of molecular crystalline polymorphs in which the linear CO_2 configuration is preserved.[4,5] At even higher pressures, CO_2 transforms into an extended covalent solid, in which carbon atoms adopt tetrahedral coordination, each bonded to four oxygen atoms.[6–9]

Atmospheric CO_2 is consumed during the chemical weathering of calcium-bearing silicate minerals, releasing calcium and bicarbonate ions that subsequently precipitate as calcium carbonates ($CaCO_3$), thereby forming a long-term carbon sink.[2] Surface carbonates, which contain trigonal [CO_3] groups, are transported into the Earth's mantle along with subducting oceanic lithosphere, exposing them to progressively higher pressures and temperatures.[1] Under these conditions, carbonates could potentially react with surrounding silicate minerals to form high-pressure carbonate-silicate assemblages. However, CO_2- and SiO_2-bearing compounds exhibit markedly different chemical behaviors at typical subduction P–T conditions, which hinders the formation of stable calcium silicate-carbonate phases due either to the thermodynamic stability of separate carbonate and silicate phases or to kinetic limitations. Consequently, despite the coexistence of CO_2, carbonates, and silicates under extreme conditions, the formation of distinct calcium silicate-carbonate compounds seems to be largely restricted to specific geological settings. To date, only three naturally occurring calcium silicate-carbonate minerals—tilleyite, $Ca_5(Si_2O_7)(CO_3)_2$,[10–12] spurrite $Ca_5(SiO_4)_2(CO_3)$[11,13] and galuskinite $Ca_7(SiO_4)_3(CO_3)$[14]—have been documented, all forming in highly localized environments where silicate and carbonate components coexist in appropriate ratios under relatively low temperatures and pressures, with sufficient

[*] B. D. Botan-Neto, Prof. Dr. D. Santamaria-Perez
Departamento de Física Aplicada – ICMUV, MALTA Consolider Team, Universitat de València, Avda. Vicente Andrés Estelles 22, Burjassot, Valencia 46100, Spain
E-mail: bebone@uv.es
david.santamaria@uv.es

J. Bungarten, Dr. L. Bayarjargal, Prof. Dr. B. Winkler
Institut für Geowissenschaften, Goethe-Universität Frankfurt, Altenhöferallee 1, 60438 Frankfurt am Main, Germany

Prof. Dr. A. Otero-de-la-Roza
Departamento de Química Física y Analítica, Facultad de Química, MALTA Consolider Team, Universidad de Oviedo, C/ Julián Clavería 8, Campus Universitario de El Cristo, Oviedo 33006, Spain

Dr. B. Wang
Deutsches Elektronen-Synchrotron DESY, Notkestraße 85, 22607 Hamburg, Germany

Additional supporting information can be found online in the Supporting Information section

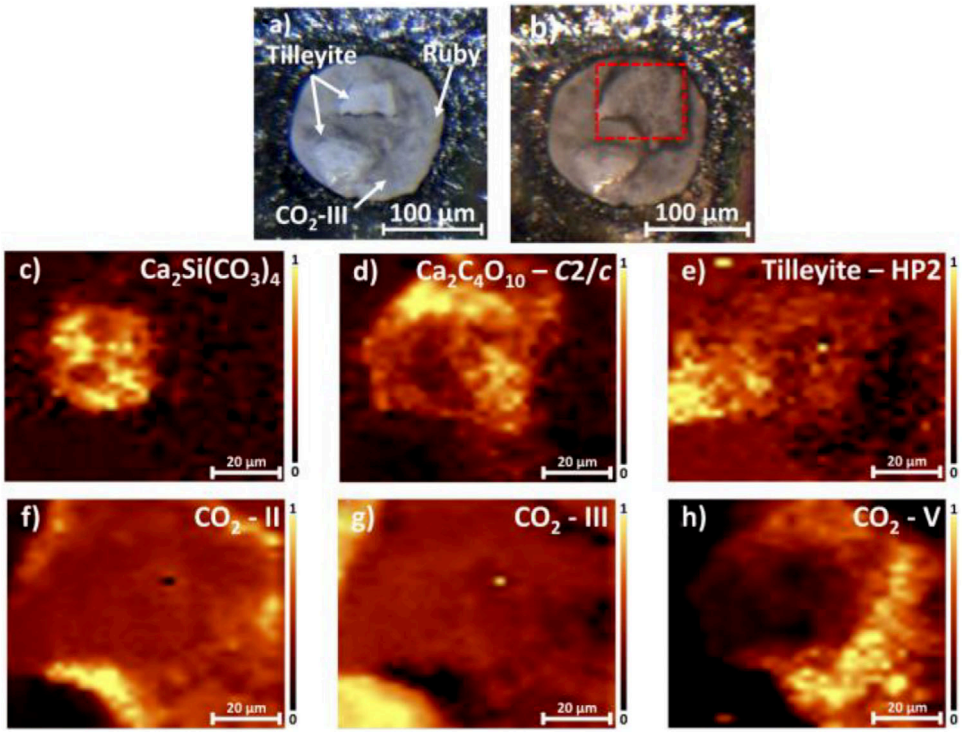

Figure 1. a) Sample chamber of the DAC containing two tilleyite crystals, ruby as a pressure gauge, and CO_2-III as the reactive medium at 39.5 GPa before laser heating. b) Sample chamber of the DAC at 39.5 GPa after laser heating. The red dashed box highlights the Raman mapping area of the heated crystal. c–h) 2D Raman maps after laser heating showing the phase distribution of: (c) $Ca_2Si(CO_3)_4$ (~1214 cm^{-1}), (d) $Ca_2C_4O_{10}$ – C2/c (~488 cm^{-1}), (e) tilleyite HP2 phase (~1176 cm^{-1}), (f) CO_2-II (~388 cm^{-1}), (g) CO_2-III (~360 cm^{-1}), and (h) CO_2-V (~777 cm^{-1}) in the framed rectangular area depicted in (b).

fluid mobility to enable ion exchange and crystallization. The three silicate-carbonate minerals above feature carbonate [CO_3] groups and [SiO_4] tetrahedra, the latter either isolated or forming pyrosilicate anions. Because they do not share oxygen atoms, the carbonate and silicate components in these minerals are chemically distinct and structurally similar to the same moieties found in pure carbonates and pure silicates. A recent study reported the polymerization between carbonate and silicate groups in carbon-bearing silica glasses above 8 GPa and discussed its implications for carbon-bearing dense silicate melts.[15]

Numerous groups have extensively searched for stable silicon carbonate phases across a range of P–T conditions.[16–23] Within the SiO_2–CO_2 system, only a disordered silicon carbonate compound has been experimentally observed, formed via the reaction of the oxides at approximately 20 GPa and 900 K.[16] The structure of this phase was only partially characterized after temperature quenching, and its detailed atomic arrangement remains unknown, although it has been predicted by evolutionary algorithm calculations.[22,23] In the CaO–SiO_2–CO_2 system, the formation of a dense post-tilleyite structure has been reported, featuring a variety of cation sites capable of accommodating atoms of differing sizes.[12] Post-tilleyite is a silicate-carbonate phase also comprising trigonal planar [CO_3] and tetrahedral [SiO_4] units. A recent preprint reports the synthesis of $CaSi[C_2O_7]$, a high-pressure high-temperature phase (122(2) GPa, 2800(200 K) built from [CO_4] tetrahedra, which form [C_2O_7] units, and [SiO_6] octahedra.[24] By contrast, the DFT-predicted SiC_2O_6 phase contains distorted [SiO_6] octahedra alongside [CO_3] groups,[22,23] but this structure has not yet been experimentally confirmed. Investigating the chemistry of these compositionally simple systems is of significant interest not only for materials science—owing to the potential formation of novel materials with unique physical properties—but also for Earth and planetary sciences, where such phases could represent accessory carbonates in the mantle.

Here, we present the results of high-pressure single-crystal X-ray diffraction (SCXRD) experiments on quenched high-temperature dense samples, combined with Raman spectroscopy measurements and density functional theory (DFT) calculations, which demonstrate the formation of a silicon carbonate phase, $Ca_2Si(CO_3)_4$. This new phase is unique in several aspects. First, it features silicon atoms in octahedral coordination, which, to the best of our knowledge, represents the first experimental observation of sixfold coordinated (octahedral [SiO_6] units) silicon in a carbonate, with the exception of the mineral thaumasite,[25,26] $Ca_3Si(OH)_6(CO_3)(SO_4)\cdot 12H_2O$, which forms in aqueous environments and contains [$Si(OH)_6$] octahedra. Second, the structure of $Ca_2Si(CO_3)_4$ contains [CO_3] triangular groups, where the oxygen atoms are shared with the silica network, constituting the first crystalline example of oxygen-sharing between carbonate and silicate groups observed. Importantly, $Ca_2Si(CO_3)_4$ can be quenched to ambient conditions, where it remains as a metastable phase. During these experiments,

we also identified a novel dense polymorphic form of calcium carbonate, $Ca_2(C_4O_{10})$, in which tetrahedral $[CO_4]$ units assemble into $[C_4O_{10}]^{4-}$ anions that are topologically analogous to P_4O_{10} phosphorus oxide.

Results and Discussion

Phase Identification and Mapping

The pressure in the diamond anvil cell (DAC) was increased up to 39.5(4.0) GPa, at which point tilleyite appeared in its second, yet unresolved high-pressure polymorph (HP2)[12] and CO_2 was transformed to phase III (Figure 1a). Upon laser heating to 2600(260) K and subsequent temperature quench, the sample chamber was as shown in Figure 1b. Raman mapping of the heated crystal was then performed to determine the spatial distribution of phases and to identify possible chemical reaction products. Six distinct phases were detected in the Raman map (Figure 1c–h): two previously unknown phases (Figure 1c, d), tilleyite HP2 (Figure 1e), and CO_2-II, III, and V (Figure 1f–h), with Raman peaks located approximately at 1214, 488, 1176, 388, 360, and 777 cm^{-1}, respectively.

After establishing the phase distribution, XRD mapping was carried out to locate the most suitable regions for probing the crystalline domains of the unknown phases. As discussed below, these correspond to (i) a new calcium silicon double carbonate ($Ca_2Si(CO_3)_4$) and (ii) a new polymorph of calcium tetracarbonate ($Ca_2C_4O_{10}$), featuring sp^3 hybridized carbon. Structural refinement of the phases was subsequently undertaken in detail.

Crystal Structure of $Ca_2Si(CO_3)_4$

Although crystalline domains smaller than 1×1 μm^2 formed after laser heating, the structure was successfully solved by synchrotron single-crystal X-ray diffraction using multigrain data analysis techniques. At 39.5 GPa, the anhydrous dicalcium silicon tetracarbonate ($Ca_2Si(CO_3)_4$), crystallizes in the monoclinic space group $P2_1/c$. The refined lattice parameters at 39.5 GPa are: a = 4.1653(5) Å, b = 14.2462(16) Å, c = 5.2244(17) Å, β = 101.27(2)°, with a unit-cell volume of V = 304.04(11) $Å^3$, Z = 2, and a calculated density of ρ = 3.804 $g{\cdot}cm^{-3}$. The crystal structure is shown in Figure 2. Details of the XRD data collection and refinement results are provided in Table 1. Experimental and calculated structural data at 39.5 GPa are provided in Tables S2–S4.

The structure of $Ca_2Si(CO_3)_4$ comprises chains of isolated $[SiO_6]$ octahedra bridged by carbonate groups forming SiO_6–CO_3–SiO_6 linkages along the [100] direction. Two crystallographically independent and distorted carbonate groups, $[C(1)O_3]$ and $[C(2)O_3]$, are present. The $[C(1)O_3]$ planar units share two of their oxygen atoms with adjacent $[SiO_6]$ octahedra, establishing the connectivity that defines the chains, whereas the $[C(2)O_3]$ units share only one corner. These carbonate groups are tilted by 26.4° and 23.5° relative to the *ab* plane, respectively. The coordination environment of the Ca atoms was evaluated using the atomic Voronoi–Dirichlet polyhedral analysis[27] implemented in the ToposPro software.[28,29] The coordination number was determined from the major faces of the Voronoi–Dirichlet polyhedra, which correspond to direct neighbors. Minor faces were neglected, as the present structural description is restricted to the first coordination sphere. The Ca atoms form double $[CaO_{10}]$ bicapped square-antiprismatic polyhedra arranged along the *bc*-plane, with two oxygen atoms shared between adjacent $[CaO_{10}]$ units. The $[SiO_6]$ octahedra link to the $[CaO_{10}]$ units through two shared edge oxygen atoms, thereby connecting neighboring double units within the *bc*-plane.

The $[CaO_{10}]$ unit exhibits an average Ca—O bond length of 2.368 Å, with eight individual bond lengths ranging from 2.163(3) to 2.357(4) Å and two bond lengths of 2.633(3) and 2.844(3) Å, a total polyhedral volume of 27.428 $Å^3$ and an effective coordination number (ECoN)[30,31] of 8.21. In contrast, the $[SiO_6]$ octahedra display an average Si—O bond length of 1.719 Å, with individual bond lengths between 1.701(3) and 1.736(3) Å, a polyhedral volume of 6.757 $Å^3$ and a distortion index of 0.007, which indicates a nearly ideal octahedral geometry The two types of carbonate groups, on the other hand, are highly irregular. In the $[C(1)O_3]$ units, one C—O bond is short (1.223(5) Å) while the other two are longer (1.280(5) and 1.298(5) Å), whereas in the second type of carbonate units $[C(2)O_3]$ two bonds are short (1.240(5) and 1.242(5) Å) and one is long (1.330(5) Å). Atoms-in-molecules delocalization indices,[32] which effectively reflect bond orders, were calculated using maximally localized Wannier functions.[33] The pattern of bond lengths in the two carbonates correlates with their respective C—O—Ca and C—O—Si connectivity and agrees with the calculated delocalization indices (DI) between the carbon and oxygen atoms. For C1, two bonds have higher DI than the third (approximately 0.95 and 0.75 at 39.5 GPa), corresponding to the bond whose oxygen is bonded to Si. For C2, one bond exhibits a large DI and the other two smaller values (approximately 1.05 and 0.82), consistent with a carbonate group sharing two vertices with adjacent Si atoms. The carbon atoms of the CO_3 groups connected to two Si atoms are slightly less positively charged, according to calculations (atomic charge of 2.19), than those connected to one Si atom (2.22).

Following structural characterization, the DAC was decompressed to ambient pressure to evaluate the stability of the newly synthesized high-pressure compound. The double carbonate remains stable at ambient conditions, retaining its monoclinic crystal structure (space group $P2_1/c$) and confirming its recoverable nature. The refined lattice parameters at ambient pressure are: a = 4.3946(2) Å, b = 15.5347(8) Å, c = 5.8337(14) Å, β = 104.155(12)°, with a unit-cell volume of V = 386.17(10) $Å^3$, Z = 2, and a calculated density of ρ = 2.995 $g{\cdot}cm^{-3}$. Table 1 summarizes the crystal data, data collection, and structure refinement parameters for $Ca_2Si(CO_3)_4$ obtained experimentally at high pressure and at ambient pressure, together with crystallographic data calculated from DFT, which show excellent agreement with the experimental results. Experimental and calculated structural data at room pressure are provided in Tables S5–S7.

The compressional behavior of the newly discovered double carbonate, $Ca_2Si(CO_3)_4$, was investigated to assess

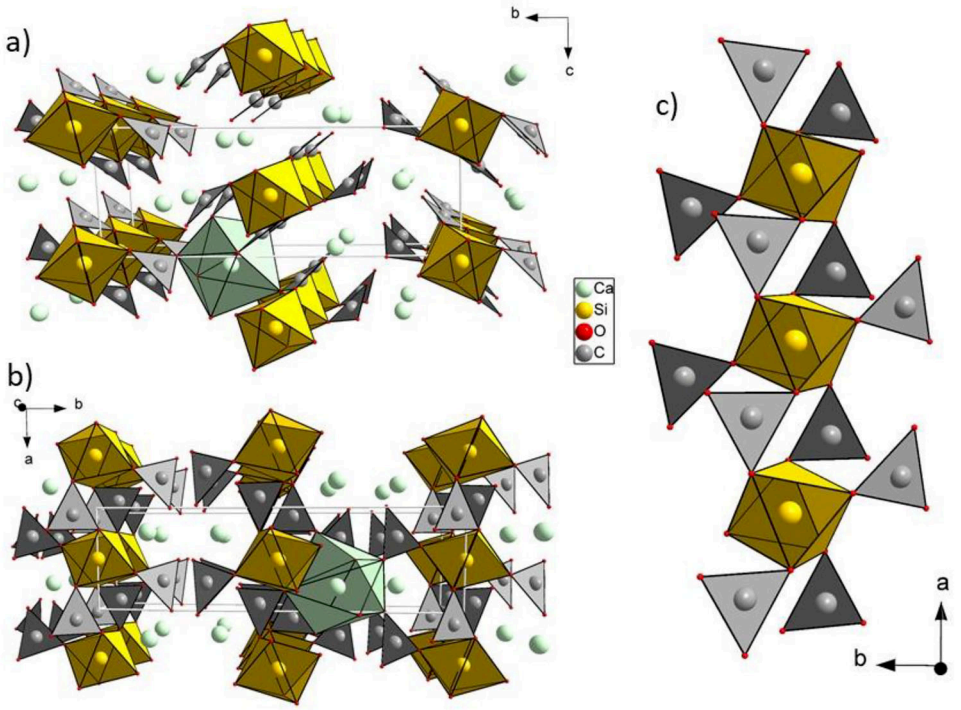

Figure 2. Projections of the $Ca_2Si(CO_3)_4$ crystal structure at 39.5 GPa along the a) *a*-axis, b) *c*-axis, and c) *c*-axis, highlighting the SiO_6–CO_3–SiO_6 linkages along the [100] direction. Calcium (Ca), silicon (Si), oxygen (O), and carbon (C) atoms are shown in light green, yellow, red, and gray, respectively.

its compressibility and structural stability under pressure. Figure 3 illustrates the evolution of the unit-cell volume as a function of pressure (**a**) and the pressure dependence of the lattice parameters (**b**). Since only 2 experimental data points are available, the bulk modulus and axial compressibility were primarily determined from DFT-calculated data. A third-order Birch–Murnaghan (BM3) equation of state was fitted to the DFT data using the EoSFit7-GUI software.[34] The fit yielded a zero-pressure volume (V_0) of 391.2(4) Å^3, a bulk modulus (K_0) of 73.8(14) GPa, and a first pressure derivative (K'_0) of 5.32(10). Since the DFT-calculated structural parameters showed excellent agreement with the experimental measurements, the bulk modulus was also estimated using the two experimental pressure points available. For this purpose, the zero-pressure volume was fixed to the experimental value obtained under ambient conditions, and the first pressure derivative was constrained to the DFT-derived value ($K'_0 = 5.32$), resulting in a bulk modulus of $K_0 = 88(9)$ GPa. The bulk modulus of the double carbonate is consistent with previously reported values for silicate-carbonate phases with tetrahedrally coordinated silicon, being 77(1) GPa for spurrite,[13] 80(2) GPa for tilleyite,[12] and 83(3) GPa for post-tilleyite,[12] demonstrating a strong correlation in compressibility behavior between the new calcium silicon carbonate and early known carbonate-silicate phases. Moreover, the bulk modulus of this compound lies within the range typically observed for common carbonates and silicates, including calcite ($K_0 = 69(2)$ GPa),[35] aragonite ($K_0 = 63(2)$ GPa),[36] coesite ($K_0 = 94(1)$ GPa),[37] and larnite ($K_0 = 103(2)$ GPa),[38] The principal axes of compression and their corresponding compressibilities were determined using PASCal v2.2.0,[39] based on the DFT-optimized structural data. The approximate crystallographic directions of maximum, intermediate, and minimum compressibility were found to be [$\bar{1}$ 0 2], [0 1 0], and [12, 0, 5], with linear compressibilities of $\kappa_1 = 3.65(3) \times 10^{-3}$ GPa^{-1}, $\kappa_2 = 2.26(1) \times 10^{-3}$ GPa^{-1}, and $\kappa_3 = 0.53(2) \times 10^{-3}$ GPa^{-1}, respectively.

Raman spectroscopy provides additional insights into the bonding characteristics of $Ca_2Si(CO_3)_4$ under compression and after decompression. Group-theoretical analysis based on the point group C_{2h} reveals a total of 114 vibrational modes at the Brillouin-zone center (Γ), consisting of 111 optical and three acoustic modes. Among these, 54 optical modes are Raman-active and are distributed according to $\Gamma_{Raman} = 27A_g + 27B_g$.[40–43] Experimental and DFT-calculated Raman spectra of $Ca_2Si(CO_3)_4$ at 39.5 GPa are shown in Figure S1. No pure Raman spectrum of the phase could be obtained, likely due to the limited spectrometer resolution, the submicrometric size of the crystalline domains, and partial spectral overlap with coexisting phases. In this context, several spurious peaks arising from coexisting phases were identified and labeled accordingly. From the experimental Raman spectra, 13 Raman-active modes were observed at approximately 145, 216, 254, 305, 702, 813, 840, 892, 1214, 1247, 1481, 1706, and 1756 cm^{-1}. Using Critic2[44,45] and DFT calculations, these modes could be attributed to the characteristic vibrations of the new $Ca_2Si(CO_3)_4$ phase. The low-frequency region (145–305 cm^{-1}) corresponds to lattice modes involving Ca^{2+} cations and the collective motion of

Table 1: Crystal data, data collection, and structure refinement parameters for $Ca_2Si(CO_3)_4$ obtained experimentally from single-crystal X-ray diffraction at 39.5 GPa and ambient pressure, together with crystallographic data calculated from DFT at 39.5 and 0 GPa.

	Experimental		DFT	
Pressure (GPa)	39.5	10^{-4}	39.5	0
Crystal data				
CCDC number	2494285	2494286	–	–
Empirical formula	$Ca_2SiC_4O_{12}$			
Formula weight [g·mol^{-1}]	348.29			
Crystal system	Monoclinic			
Space group (number)	$P2_1/c$ *(14)*			
a **[Å]**	4.1653(5)	4.3946(2)	4.13841	4.40532
b **[Å]**	14.2462(16)	15.5347(8)	14.17967	15.69894
c **[Å]**	5.2244(17)	5.8337(14)	5.16065	5.90113
β **[°]**	101.27(2)	104.155(12)	98.14	104.47
Volume [Å^3]	304.04(11)	386.17(10)	299.99	394.37
Z	2			
ρ_{calc} **[g.cm^{-3}]**	3.804	2.995	3.86	2.93
μ **[mm^{-1}]**	0.217	0.171	–	–
Data collection				
F**(000)**	348		–	–
Radiation	Synchrotron ($\lambda = 0.2904$)		–	–
2*θ* Range [°]	4.0704 to 28.006	3.906 to 27.994	–	–
Index Ranges	$-6 \le h \le 6$ $-23 \le k \le 22$ $-6 \le l \le 5$	$-7 \le h \le 7$ $-25 \le k \le 23$ $-5 \le l \le 5$	–	–
Reflections collected	1397	1831	–	–
Independent reflections	673	833	–	–
Crystal structure refinement				
Data/restraints/parameters	673/0/88	833/0/88	–	–
Goodness-of-fit on F^2	1.152	1.006	–	–
Final *R* Indexes [I ≥ 2*σ*(I)]	$R_1 = 0.0453$ $wR_2 = 0.1320$	$R_1 = 0.0421$ $wR_2 = 0.0982$	–	–
Final *R* Indexes [All Data]	$R_1 = 0.0528$ $wR_2 = 0.1362$	$R_1 = 0.0598$ $wR_2 = 0.1044$	–	–
$\Delta\rho_{max}/\Delta\rho_{min}$ [eÅ^{-3}]	0.53/−0.94	0.61/−0.40	–	–

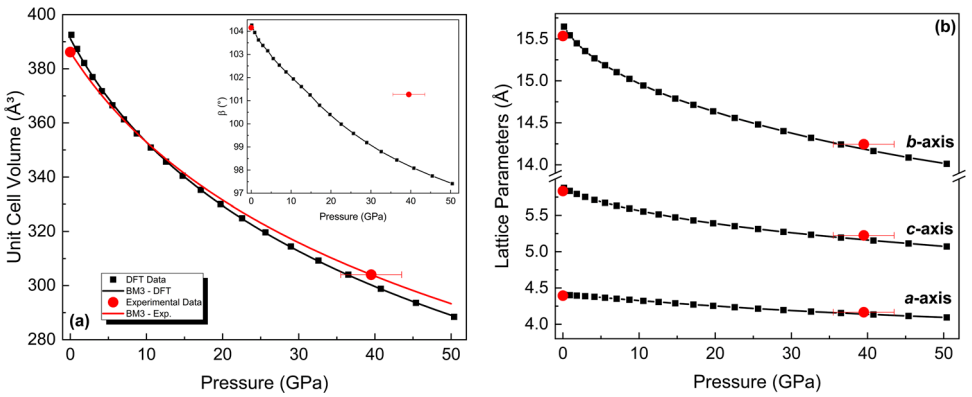

Figure 3. a) Pressure dependence of the $Ca_2Si(CO_3)_4$ unit-cell volume up to 50 GPa. DFT-calculated data (black squares) and SCXRD experimental data (red circles) are shown, with solid lines representing 3rd-order Birch–Murnaghan fits. The inset shows the evolution of the β angle with pressure. b) Pressure dependence of the $Ca_2Si(CO_3)_4$ lattice parameters.

[SiO_6] and [CO_3] units. The peak at 702 cm^{-1} is assigned to the combined O—Si—O in-plane bending (ν_4) and O—C—O in-plane bending (ν_4) modes. The peaks between 813 and 892 cm^{-1} correspond to O—Si—O symmetric stretching (ν_1) coupled with O—C—O out-of-plane bending (ν_2). The peak at 1214 cm^{-1} is attributed to O—Si—O asymmetric stretching (ν_3), whereas the 1247 cm^{-1} peak corresponds to O—C—O symmetric stretching (ν_1). Finally, the high-frequency region (1481–1756 cm^{-1}) is dominated by O—C—O asymmetric stretching (ν_3) vibrations.

Crystal Structure of $Ca_2C_4O_{10}$

Three types of carbonate groups exhibiting two distinct hybridization states are currently known. The first corresponds to the "conventional" carbonate group, consisting of nearly planar trigonal $[CO_3]^{2-}$ units with sp^2-hybridized carbon atoms.[46,47] Each group contains a central carbon atom bonded to three surrounding oxygen atoms, with typical C—O bond lengths of approximately 1.30 Å and O—C—O bond angles close to 120°. These sp^2-hybridized carbonate groups constitute the fundamental building units of the most abundant and stable carbonates in the Earth's crust—such as magnesite ($MgCO_3$), calcite ($CaCO_3$), and dolomite ($CaMg(CO_3)_2$)—which together account for nearly 90% of the total carbonate content of this layer.[48–51] The second and most recently discovered type corresponds to the pyrocarbonate group, which also exhibits sp^2 hybridization. It consists of $[C_2O_5]^{2-}$ units formed by the polymerization of two $[CO_3]^{2-}$ groups that share a common oxygen atom, resulting in a C—O—C linkage between adjacent carbonate units.[52–54] Pyrocarbonate compounds have been synthesized for the first time only recently.[55] Since then, several pyrocarbonate salts have been successfully synthesized.[56–59] The third type corresponds to the tetrahedrally coordinated carbonate group $[CO_4]^{4-}$, which exhibits a tetrahedral geometry with sp^3-hybridized carbon atoms.[60–63] These units are stable under pressures and temperatures corresponding to the Earth's transition zone and the uppermost lower mantle (>35 GPa and 2000–3000 K).[64, 65] Under ambient conditions, however, sp^3 hybridization is energetically unfavorable due to the very small size of the C^{4+} cation relative to O^{2-}, which leads to excessive O—O steric repulsion.[66] Under high-pressure conditions, carbon stabilizes in the sp^3-hybridized state, adopting a coordination environment analogous to silicon in silicates. This increased coordination confers a volumetric advantage that offsets steric repulsion. Tetrahedrally coordinated carbonate groups may occur as isolated tetrahedra, dimers, rings, pyramidal clusters, or extended chains, with the tetracarbonate group represented by the pyramidal $[C_4O_{10}]^{4-}$ unit.[60,61,65,67–70]

Calcium tetracarbonate ($Ca_2C_4O_{10}$) has previously been reported experimentally in the literature in two different space groups at 34(2) GPa: a tetragonal phase with space group $I\bar{4}2d$ and a cubic phase with space group $Fd\bar{3}m$.[64] The tetragonal structure can be described as a slightly distorted derivative of the cubic one, with the relationship $a_{cubic} = \sqrt{2}\, a_{tetragonal}$. Density functional theory (DFT) calculations

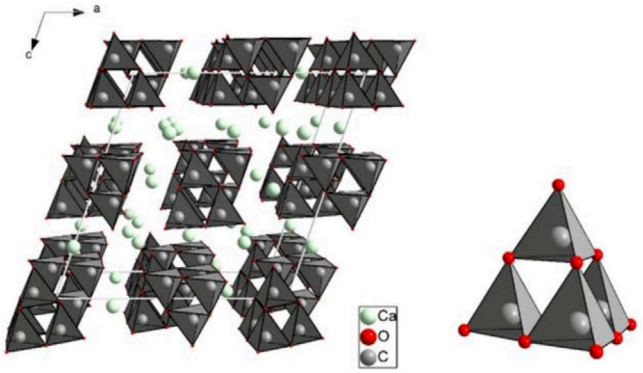

Figure 4. Projection of the $Ca_2[C_4O_{10}]$ crystal structure along the *b*-axis **(left)** at 39.5 GPa, and the tetrahedral $[C_4O_{10}]$ unit **(right)**. Calcium (Ca), oxygen (O), and carbon (C) atoms are shown in light green, red, and gray, respectively.

indicate that the tetragonal phase is energetically more favorable than the cubic form. In the present work, we identified $Ca_2C_4O_{10}$ crystallizing in the monoclinic space group *C*2/*c*. At 39.5 GPa, the refined lattice parameters are: $a = 11.993(8)$ Å, $b = 7.0949(9)$ Å, $c = 12.316(5)$ Å, $\beta = 109.07(7)°$, with a unit-cell volume of $V = 990.4(9)$ Å^3, $Z = 16$, and a calculated density of $\rho = 3.866$ g·cm^{-3}. The crystal structure is shown in Figure 4. It comprises three crystallographically independent calcium polyhedra: two [CaO_{10}] bicapped square antiprism and one distorted [CaO_{12}] icosahedron. These polyhedra are corner-shared through oxygen atoms belonging to polymerized orthocarbonate $[CO_4]^{4-}$ groups, which form distorted pyramidal $[C_4O_{10}]^{4-}$ units with sp^3-hybridized carbon atoms.

In projection onto the *ac*-plane, the cationic framework forms a square-grid topology, which can be compared to a tic-tac-toe pattern. In this analogy, the three-by-three grid (#) represents the cationic framework: Ca atoms occupy the grid intersections (forming the #), while the tetrahedral $[C_4O_{10}]$ units are positioned at the "X" and "O" sites, completing the planar representation of the framework. Table 2 summarizes the crystal data, data collection, and structure refinement parameters for $Ca_2C_4O_{10}$ obtained experimentally at high pressure. Structural data, including atomic coordinates and isotropic and anisotropic displacement parameters, are provided in Tables S8 and S9.

DFT-relaxed structural optimization of the experimentally found *C*2/*c* phase results in a trigonal $R\bar{3}c$ crystal structure for the newly identified polymorph of calcium tetracarbonate. Phonon calculations performed in a 2 × 2 × 1 supercell at the DFT equilibrium structure corresponding to the closest point of the volume grid (39.9 GPa) yielded only positive harmonic frequencies, confirming that the $R\bar{3}c$ structure is dynamically stable. At 39.5 GPa, the DFT-obtained lattice parameters are: $a = 6.9210$ Å and $c = 34.2918$ Å, with a unit-cell volume of $V = 1456.89$ Å^3, $Z = 12$, and a calculated density of $\rho = 3.94$ g·cm^{-3}. The detailed structural data at 39.5 GPa are provided in Table S10. The experimental data set could also be solved in this trigonal setting, yielding refined lattice parameters: $a = 7.0222(9)$ Å and $c = 34.873(3)$ Å, with a unit-cell volume of $V = 1489.3(4)$ Å^3, $Z = 12$, and a calculated

Table 2: Crystal data, data collection, and structure refinement parameters for $Ca_2C_4O_{10}$ were obtained experimentally from single-crystal X-ray diffraction (SCXRD) at 39.5 GPa.

	Experimental
Pressure (GPa)	39.5
Crystal data	
CCDC number	2494194
Empirical formula	$Ca_2C_4O_{10}$
Formula weight [g.mol^{-1}]	288.20
Crystal system	Monoclinic
Space group (number)	*C*2/*c (15)*
***a* [Å]**	11.993(8)
***b* [Å]**	7.0949(9)
***c* [Å]**	12.316(5)
***β* [°]**	109.07(7)
Volume [Å^3]	990.4(9)
Z	8
ρ_{calc} [g.cm^{-3}]	3.866
μ [mm^{-1}]	0.233
Data collection	
***F*(000)**	1152
Radiation	Synchrotron ($\lambda = 0.2904$)
2*θ* range [°]	3.328 to 27.976
Index Ranges	$-13 \le h \le 14$ $-11 \le k \le 11$ $-18 \le l \le 16$
Reflections collected	2331
Independent reflections	948
Crystal structure refinement	
Data/restraints/parameters	948/0/97
Goodness-of-fit on F^2	1.101
Final *R* Indexes [I ≥ 2*σ*(I)]	$R_1 = 0.0633$ $wR_2 = 0.1624$
Final *R* Indexes [All Data]	$R_1 = 0.0969$ $wR_2 = 0.1772$
$\Delta\rho_{max}/\Delta\rho_{min}$ [eÅ^{-3}]	0.99/−0.57

density of $\rho = 3.86$ g·cm^{-3}, but slightly worse figure of merit. Notably, the experimentally observed monoclinic *C*2/*c* cell displays a pseudo-rhombohedral metric, as expected for a weakly distorted trigonal lattice. The detailed transformation relating the monoclinic and trigonal descriptions is discussed in the Supporting Information.

The $Fd\bar{3}m$ structure reported by König et al., [64] represents the aristotype from which all known CaC_2O_5 polymorphs can be derived. The previously reported $I\bar{4}2d$ phase[64] and the *C*2/*c* and $R\bar{3}c$ structures discussed in this work arise from symmetry-lowering distortions of this cubic parent structure while preserving the $[C_4O_{10}]^{4-}$ motif. The corresponding group–subgroup relationships are summarized in Figure S2 through a Bärnighausen tree. This analysis shows that the tetragonal polymorph arises directly from the cubic aristotype, whereas the trigonal $R\bar{3}c$ structure—and, subsequently, the monoclinic *C*2/*c* variant—derive from a distinct branch of the same cubic parent. Consequently, the polymorphs discussed here correspond to independent distortion pathways of the cubic aristotype.

Upon decompression, the phase was found to be unrecoverable at ambient conditions. Nevertheless, DFT calculations allow for the estimation of its elastic properties and the assessment of structural stability under pressure, in comparison with existing polymorphs and analogous $M_2[C_4O_{10}]$ compounds (M = Ca, Fe, Cd). The evolution of the unit-cell volume with pressure and the pressure dependence of the lattice parameters are shown in Figures S3 and S4, respectively. A third-order Birch–Murnaghan fit yielded a zero-pressure volume (V_0) of 1210.53(18) Å^3, a bulk modulus (K_0) of 104.2(3) GPa, and a first pressure derivative (K'_0) of 4.90(2). The principal crystallographic directions of compression were found to be [100], [010], and [103], with linear compressibilities of $\kappa_1 = 1.83(1) \times 10^{-3}$ GPa^{-1}, $\kappa_2 = 1.83(1) \times 10^{-3}$ GPa^{-1}, and $\kappa_3 = 1.81(2) \times 10^{-3}$ GPa^{-1}, respectively. The nearly identical values indicate that the crystal exhibits essentially isotropic compressibility.

Table 3 summarizes the DFT equation-of-state (EoS) parameters for the $M_2[C_4O_{10}]$ compounds (M = Ca, Cd, Fe). For completeness and future reference, a second-order BM (BM2) fit for the present work is also included in the table. For monoclinic calcium tetracarbonate, the bulk modulus falls within the range of other sp^3 calcium carbonates.[35,36] Calcium orthocarbonate Ca_2CO_4, for instance, has a K_0 value of 108(1) GPa.[68] The tetragonal polymorph of calcium tetracarbonate, with $K_0 = 93.4(4)$ GPa, exhibits a bulk modulus approximately 10% lower than that of the monoclinic phase. This difference can reasonably be attributed to variations in cation coordination, from a 10-fold coordination in the monoclinic structure to a 12-fold coordination in the tetragonal polymorph. Cadmium tetracarbonate ($Cd_2C_4O_{10}$)[71] and iron tetracarbonate ($Fe_2C_4O_{10}$),[72] structural analogues of $Ca_2C_4O_{10}$ reported previously in the literature, display distinct compressibilities. $Cd_2C_4O_{10}$ exhibits a bulk modulus ($K_0 = 112.2(5)$ GPa) approximately 8% higher than monoclinic $Ca_2C_4O_{10}$, while $Fe_2C_4O_{10}$ presents the bulk modulus ($K_0 = 127(3)$ GPa) roughly 22% higher. These trends reinforce the general observation that the bulk moduli of carbonates containing $[C_4O_{10}]^{4-}$ units tend to increase with decreasing cation radius, which is directly related to the fact that the $[CO_4]$ units are largely incompressible, and the bulk moduli mainly depend on the $[MO_x]$ polyhedral compressibility.

Raman spectroscopy was performed for the new calcium tetracarbonate polymorph. Group-theoretical analysis based on the point group C_{2h} reveals a total of 192 vibrational modes at the Brillouin-zone center (Γ), consisting of 189 optical and three acoustic modes. Among these, 93 optical modes are Raman-active and are distributed according to $\Gamma_{Raman} = 46A_g + 47B_g$.[40–43] Experimental and DFT-calculated Raman spectra of $Ca_2C_4O_{10}$ at 39.5 GPa are shown in Figure S5. No pure Raman spectrum of the phase could be obtained. Eight Raman-active modes observed at approximately 450, 488, 593, 622, 745, 768, 1004, and 1025 cm^{-1} were assigned to the CaC_2O_4 phase. The modes at 450, 488, 593, 745, and 768 cm^{-1} correspond to O─C─O in-plane bending (ν_4), while those at 622, 1004, and 1025 cm^{-1} correspond to O─C─O symmetric stretching (ν_1). Four of the eight observed Raman modes (450, 622, 745, and 768 cm^{-1}) show excellent agreement with previously reported modes for the tetragonal structure at 497,

Table 3: Comparison of Birch–Murnaghan (BM) equation-of-state (EoS) parameters for $M_2[C_4O_{10}]$ compounds (M = Ca, Cd, Fe), including space group symmetry, zero-pressure volume (V_0), bulk modulus (K_0), and its first pressure derivative (K'_0). Table updated from Kovalev et al.[72] Licensed under CC-BY 4.0 (https://creativecommons.org/licenses/by/4.0/). [Correction added on January 28, 2026, after first online publication: Table 3 has been updated.]

Compound	Space group	Data	V_0 (Å^3)	K_0 (GPa)	K'_0	Ref.
$Ca_2C_4O_{10}$	*C*2/*c*	DFT – BM2	1202.9(14)	120.2(11)	4.0	This work
		DFT – BM3	1210.53(18)	104.2(3)	4.90(2)	
$Ca_2C_4O_{10}$	$I\bar{4}2d$	DFT – BM2	611(3)	110(3)	4.0	[64]
		DFT – BM3	616.7(2)	93.4(4)	4.83(2)	
$Cd_2C_4O_{10}$	$Fd\bar{3}m$	DFT – BM2	1186.4(6)	132(3)	4.0	[71]
		DFT – BM3	1196.8(8)	112.2(5)	5.21(3)	
$Fe_2C_4O_{10}$	$Fd\bar{3}m$	DFT – BM2	1084(4)	152(3)	4.0	[72]
		DFT – BM3	1092(2)	127(3)	4.93(12)	
		EXP – BM2	1059(17)	160(18)	4.0	

631, 751, and 773 cm^{-1},[64] respectively. As noted above, the crystal structure of the new tetracarbonate is not recoverable at ambient conditions.

The crystal structures of calcium tetracarbonate and calcium silicon carbonate were successfully determined and described in detail. However, the HP2 phase of tilleyite, identified during Raman mapping, could not be observed in the SCXRD experiments and therefore remains structurally unresolved. The following section presents a DFT-based thermodynamic and energetic analysis of the relevant systems, including carbon dioxide (CO_2), silica (SiO_2), calcium carbonate ($CaCO_3$), calcium oxide (CaO), and tilleyite, as well as the decomposition pathways of the newly observed calcium silicon carbonate phase.

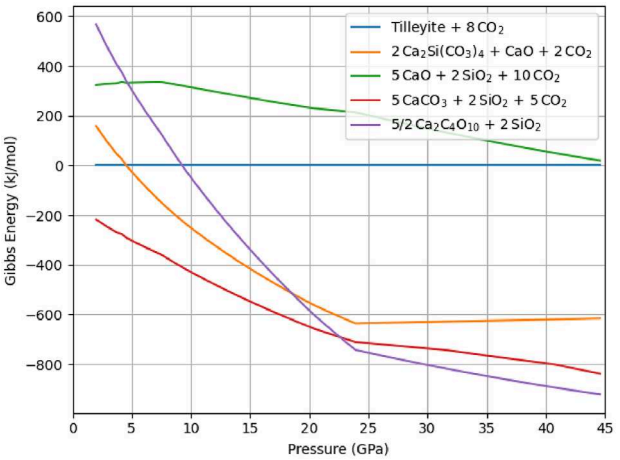

Figure 5. DFT-calculated Gibbs energy as a function of pressure at 300 K, illustrating the relative thermodynamic stability of tilleyite + CO_2 compared to $Ca_2Si(CO_3)_4$, $Ca_2(C_4O_{10})$, and the combinations of their corresponding oxides (CaO, CO_2, and $CaCO_3$). Color coding: solid blue line – tilleyite + 8 CO_2; orange line – 2 $Ca_2Si(CO_3)_4$ + CaO + 2 CO_2; green line – 5 CaO + 2 SiO_2 + 10 CO_2; red line – 5 $CaCO_3$ + 2 SiO_2 + 5 CO_2; purple line – 5/2 $Ca_2(C_4O_{10})$ + 2 SiO_2. The pressure range has been restricted to remove the zones where the quasiharmonic approximation behaves spuriously.

Thermodynamic and Energetic Stability

To evaluate the thermodynamic stability of $Ca_2Si(CO_3)_4$ and $Ca_2(C_4O_{10})$ with respect to their possible decomposition into oxides, we calculated the equations of state (EoS) in the static approximation (no vibrations) for carbon dioxide (CO_2), silica (SiO_2), calcium carbonate ($CaCO_3$), calcium oxide (CaO), and tilleyite, along with the aforementioned compounds. For each system, the relevant experimentally observed crystal structures within the 0–45 GPa pressure range were considered. The enthalpy–pressure relations were constructed by identifying, at each pressure, the lowest-enthalpy phase among the candidate structures. Additional phonon frequency calculations were carried out to incorporate the effects of temperature in the quasiharmonic approximation. The details for these calculations and results for the reference oxides and carbonates are provided in the Supporting Information.

The relative stabilities of tilleyite, $Ca_2Si(CO_3)_4$, $Ca_2(C_4O_{10})$, and the combinations of their corresponding oxides (CaO, CO_2, and $CaCO_3$) are shown in Figure 5. We must note that the data in Figure 5 informs only of thermodynamic stability, not the kinetics of the different transformations. Figures 5, S11, and S12 show the stabilities at ambient temperature, in the static approximation and at 2600 K, respectively. At low pressures, 5/2 $Ca_2(C_4O_{10})$ + 2 SiO_2 is unstable relative to 2 $Ca_2Si(CO_3)_4$ + CaO + 2 CO_2, and the latter is unstable with respect to decomposition into 5 $CaCO_3$ + 2 SiO_2 + 5 CO_2. At low temperature, the thermodynamic stability of these phases undergoes a marked change around 20 GPa, where a distinct variation in the slope of the Gibbs energy–pressure curves coincides with the appearance of phase V in the CO_2 phase diagram. Above this pressure, and at low temperature, the presence of free CO_2 becomes thermodynamically disfavored, and the stable phase is 5/2 $Ca_2(C_4O_{10})$ + 2 SiO_2 up to 45 GPa. The trend depicted in Figure 5 is consistent with previous theoretical predictions of the decomposition of $Ca_2(C_4O_{10})$- $I\bar{4}2d$ below 20 GPa at ambient conditions obtained using DFT + QHA methods,[64] as well as with experimental observations showing that this phase can be synthesized from $CaCO_3$ + CO_2 at pressures above 34 GPa but reverts to the starting materials below 18 GPa.[64]

The thermodynamic stabilities in Figure 5 are also consistent with our experimental observations. A mixture of tilleyite and CO_2 was heated, acquiring enough energy to

overcome the kinetic barriers to transition to more stable phases: $Ca_2Si(CO_3)_4$ and $Ca_2C_4O_{10}$. Upon pressure release, the transformation of the latter back to its component oxides occurred. At ambient conditions, the decomposition of $Ca_2Si(CO_3)_4$ is less favorable than that of $Ca_2C_4O_{10}$ and likely kinetically hindered, hence its metastability.

Conclusion

High pressure modifies the electron density of compounds by redistributing it within and between atoms, leading to changes in bonding, orbital hybridization, and maximizing the packing efficiency of the structure. Novel phases form to minimize enthalpy, a process that typically leads to an increase in atomic coordination. High temperatures, on the other hand, are crucial to overcoming kinetic barriers that often hinder structural transformations. At ambient pressure, silicates are usually formed by either isolated or condensed [SiO_4] tetrahedra. Known silicate-carbonate minerals consist of distinct and separate [SiO_4] and [CO_3] units with no oxygen sharing between them.

The present work investigates the chemistry of the CaO–SiO_2–CO_2 system under extreme pressure and temperature conditions using a combination of Raman spectroscopy, single-crystal X-ray diffraction, and DFT calculations. The results demonstrate that a crystalline calcium silicon carbonate with the formula $Ca_2Si(CO_3)_4$ is obtained from the reaction of naturally-occurring silicate-carbonate mineral tilleyite ($Ca_5(Si_2O_7)(CO_3)_2$) with CO_2 at approximately 39.5 GPa and 2600 K, and that this novel phase can be recovered down to ambient conditions as a metastable solid. The structure of this new phase is unique: it is an oxide with sixfold-coordinated silicon, and the triangular carbonate groups share oxygen atoms with the silica network. The octahedral coordination of Si by O is favored by the oxygen coordination to the relatively more electronegative C atoms, which draw electrons out of the Si—O bonds, lengthening them, and decreasing O—O repulsion.[73] The formation of this calcium silicon carbonate also reflects a balance between the respective stabilities of three- and fourfold coordination in carbon under high pressure, as evidenced by the simultaneous synthesis of a novel monoclinic polymorph of calcium tetracarbonate, $Ca_2(C_4O_{10})$, with sp^3-hybridized carbon atoms, while exceeding the pressure required for sixfold coordination of silicon.

The structure observed in this work is an example of a new oxide chemistry in which silicates and carbonates interact, producing a unique, light, carbon-rich oxide that remains metastable at ambient conditions. At yet higher pressure, the formation of a novel phase with coexisting 4-coordinated carbon and 6-coordinated silicon has been reported.[24]

Supporting Information

The authors have cited additional references within the Supporting Information.[74–120] The supplementary material provides detailed experimental and computational methods. Further information on the single-crystal structure solution and DFT-based calculations is also included. Experimental structural data have been deposited with the Cambridge Crystallographic Data Centre (CCDC).[121]

Acknowledgements

This research was funded by the Spanish Ministry of Science, Innovation, and Universities and the Spanish State Research Agency (MICIU/AEI/10.13039/501100011033/FEDER, UE) under projects PID2021-125518NB-I00, PID2024-158791NBI00 and CNS2023-144958, as well as by the Generalitat Valenciana under projects CIAICO/2021/241 and MFA/2022/007 (funded by the European Union-Next Generation EU), and the Principality of Asturias, project IDE/2024/000726 Q2 (cofinanced by EU FEDER funds). B.D.B.N. acknowledges Generalitat Valenciana for the predoctoral contract CIGRIS/2022/202, as well as for the financial support for the research stay CIBEFP/2024/079 at the Institute of Geosciences, Goethe University Frankfurt. J.B., L.B., and B.W. gratefully acknowledge funding from the Deutsche Forschungsgemeinschaft (DFG, projects WI1232 and BA4020). We acknowledge DESY (Hamburg, Germany), a member of the Helmholtz Association (HGF), for providing experimental facilities. Part of this research was carried out at PETRA III, beamline P02.2, under beamtime proposal I-20250095. We would like to thank D. Spahr for support with the CO_2 loading system.

Conflict of Interests

The authors declare no conflict of interest.

Data Availability Statement

The data that support the findings of this study are available in the Supporting Information of this article.

Keywords: Carbonates · High-pressure chemistry · Raman spectroscopy · Silicate-carbonates · X-ray diffraction

[1] R. Dasgupta, *Rev. Mineral. Geochem.* **2013**, *75*, 183–229, https://doi.org/10.2138/rmg.2013.75.7.
[2] R. M. Hazen, R. T. Downs, L. Kah, D. Sverjensky, *Rev. Mineral. Geochem.* **2013**, *75*, 79–107, https://doi.org/10.2138/rmg.2013.75.4.
[3] A. Jarvis, P. M. Forster, *Nat. Geosci.* **2024**, *17*, 1222–1224, https://doi.org/10.1038/s41561-024-01580-5.
[4] K. Aoki, H. Yamawaki, M. Sakashita, Y. Gotoh, K. Takemura, *Science (1979)* **1994**, *263*, 356–358.
[5] V. M. Giordano, F. Datchi, *Europhys. Lett. (EPL)* **2007**, *77*, 46002, https://doi.org/10.1209/0295-5075/77/46002.
[6] A. Sengupta, C.-S. Yoo, *Phys. Rev. B* **2010**, *82*, 012105, https://doi.org/10.1103/PhysRevB.82.012105.
[7] M. Santoro, F. A. Gorelli, R. Bini, J. Haines, O. Cambon, C. Levelut, J. A. Montoya, S. Scandolo, *Proc. Natl. Acad. Sci. USA* **2012**, *109*, 5176–5179, https://doi.org/10.1073/pnas.1118791109.

[8] F. Datchi, B. Mallick, A. Salamat, S. Ninet, *Phys. Rev. Lett.* **2012**, *108*, 125701, https://doi.org/10.1103/PhysRevLett.108.125701.

[9] Y. Han, J. Liu, L. Huang, X. He, J. Li, *NPJ Quantum Mater.* **2019**, *4*, 10, https://doi.org/10.1038/s41535-019-0149-0.

[10] S. J. Lottisnatham, J. V. Smith, *Z Kristallogr Cryst. Mater.* **1970**, *132*, 288–306, https://doi.org/10.1524/zkri.1970.132.16.288.

[11] J. D. Grice, *Can. Mineral.* **2005**, *43*, 1489–1500, https://doi.org/10.2113/gscanmin.43.5.1489.

[12] D. Santamaria-Perez, J. Ruiz-Fuertes, M. Peña-Alvarez, R. Chulia-Jordan, T. Marqueño, D. Zimmer, V. Gutiérrez-Cano, S. MacLeod, E. Gregoryanz, C. Popescu, P. Rodríguez-Hernández, A. Muñoz, *Sci. Rep.* **2019**, *9*, 7898, https://doi.org/10.1038/s41598-019-44326-9.

[13] D. Santamaria-Perez, J. Ruiz-Fuertes, T. Marqueño, J. Pellicer-Porres, R. Chulia-Jordan, S. MacLeod, C. Popescu, *Inorg. Chem.* **2018**, *57*, 98–105, https://doi.org/10.1021/acs.inorgchem.7b02101.

[14] B. Lazic, T. Armbruster, V. B. Savelyeva, A. E. Zadov, N. N. Pertsev, P. Dzierżanowski, *Mineral. Mag.* **2011**, *75*, 2631–2648, https://doi.org/10.1180/minmag.2011.075.5.2631.

[15] E. J. Kim, S. K. Lee, *Geophys. Res. Lett.* **2025**, *52*, e2024GL113755, https://doi.org/10.1029/2024GL113755.

[16] M. Santoro, F. Gorelli, J. Haines, O. Cambon, C. Levelut, G. Garbarino, *Proc. Natl. Acad. Sci. USA* **2011**, *108*, 7689–7692, https://doi.org/10.1073/pnas.1019691108.

[17] M. Santoro, F. A. Gorelli, R. Bini, A. Salamat, G. Garbarino, C. Levelut, O. Cambon, J. Haines, *Nat. Commun.* **2014**, *5*, 3761, https://doi.org/10.1038/ncomms4761.

[18] D. Santamaria-Perez, C. McGuire, A. Makhluf, A. Kavner, R. Chuliá-Jordan, J. L. Jorda, F. Rey, J. Pellicer-Porres, D. Martinez-García, P. Rodriguez-Hernández, A. Muñoz, *Nat. Commun.* **2016**, *7*, 13647, https://doi.org/10.1038/ncomms13647.

[19] A. Aravindh, A. Arkundato, S. Barman, S. Baroni, B. L. Bhargava, K. R. S. Chandrakumar, W. Chen, R. Cherian, A. D. Corso, S. Datta, S. de Gironcoli, S. S. Dhayal, A. K. Dixit, S. Dutta, P. D'yachkov, C. G. Floare, N. Ganguli, S. Ganguly, R. Gebauer, S. Ghosh, P. Giannozzi, Govind, A. J. Hatt, K. P. S. S. Hembram, M. Imam, V. Jayalakshmi, C. S. Jayanthi, T. Kelkar, Anil Kumar, J. H. Lee, M.-S. Lee, et al., *Solid State Commun.* **2007**, *144*, 273–276, https://doi.org/10.1016/j.ssc.2007.09.011.

[20] C. R. S. da Silva, J. F. Justo, I. Pereyra, L. V. C. Assali, *Diam. Relat. Mater.* **2005**, *14*, 1142–1145, https://doi.org/10.1016/j.diamond.2004.12.011.

[21] A. Morales-García, M. Marqués, J. M. Menéndez, D. Santamaría-Pérez, V. G. Baonza, J. M. Recio, *Theor. Chem. Acc.* **2013**, *132*, 1308, https://doi.org/10.1007/s00214-012-1308-6.

[22] M. Marqués, A. Morales-García, J. M. Menéndez, V. G. Baonza, J. M. Recio, *Phys. Chem. Chem. Phys.* **2015**, *17*, 25055–25060.

[23] R. Zhou, B. Qu, J. Dai, X. C. Zeng, *Phys. Rev. X* **2014**, *4*, 011030.

[24] G. Aprilis, A. Pantousas, A. Aslandukova, I. Kupenko, X. Li, S. Müller, M. Hanfland, L. Dubrovinsky, A. Pakhomova, *Research Square Preprint*, **2025**, https://doi.org/10.21203/rs.3.rs-8308717/v1.

[25] R. A. Edge, H. F. W. Taylor, *Acta Cryst. B.* **1971**, *27*, 594–601, https://doi.org/10.1107/S0567740871002619.

[26] R. A. Edge, H. F. W. Taylor, *Nature* **1969**, *224*, 363–364, https://doi.org/10.1038/224363a0.

[27] B. D. Botan-Neto, D. Santamaria-Perez, L. Wedek, L. Bayarjargal, G. Bera, P. Botella, J. Pellicer-Porres, A. Otero-de-la-Roza, C. Popescu, F. G. Alabarse, *Inorg. Chem.* **2025**, *64*, 10067–10077, https://doi.org/10.1021/acs.inorgchem.5c00642.

[28] V. A. Blatov, *IUCr Newsletter* **2006**, *7*, 4–38.

[29] V. A. Blatov, A. P. Shevchenko, D. M. Proserpio, *Cryst. Growth Des.* **2014**, *14*, 3576–3586, https://doi.org/10.1021/cg500498k.

[30] M. Nespolo, *Acta Cryst. B.* **2016**, *72*, 51–66, https://doi.org/10.1107/S2052520615019472.

[31] R. Hoppe, *Z Kristallogr* **1979**, *150*, 23–52, https://doi.org/10.1524/zkri.1979.150.1-4.23.

[32] R. F. W. Bader, M. E. Stephens, *J. Am. Chem. Soc.* **1975**, *97*, 7391–7399, https://doi.org/10.1021/ja00859a001.

[33] A. Otero-de-la-Roza, Á. Martín Pendás, E. R. Johnson, *J. Chem. Theory Comput.* **2018**, *14*, 4699–4710, https://doi.org/10.1021/acs.jctc.8b00549.

[34] J. Gonzalez-Platas, M. Alvaro, F. Nestola, R. Angel, *J. Appl. Crystallogr.* **2016**, *49*, 1377–1382, https://doi.org/10.1107/S1600576716008050.

[35] G. Fiquet, F. Guyot, J.-P. Itie, *Am. Mineral.* **1994**, *79*, 15–23.

[36] M. Merlini, M. Hanfland, W. A. Crichton, *Earth Planet. Sci. Lett.* **2012**, *333–334*, 265–271, https://doi.org/10.1016/j.epsl.2012.04.036.

[37] E. Kulik, N. Nishiyama, Y. Higo, N. A. Gaida, T. Katsura, *J. Am. Ceram. Soc.* **2019**, *102*, 2251–2256, https://doi.org/10.1111/jace.16243.

[38] Z. Xiong, X. Liu, S. R. Shieh, S. Wang, L. Chang, J. Tang, X. Hong, Z. Zhang, H. Wang, *Am. Mineral.* **2016**, *101*, 277–288, https://doi.org/10.2138/am-2016-5425.

[39] M. Lertkiattrakul, M. L. Evans, M. J. Cliffe, *J Open Source Softw.* **2023**, *8*, 5556, https://doi.org/10.21105/joss.05556.

[40] E. Kroumova, M. I. Aroyo, J. M. Perez-Mato, A. Kirov, C. Capillas, S. Ivantchev, H. Wondratschek, *Phase Transitions* **2003**, *76*, 155–170, https://doi.org/10.1080/0141159031000076110.

[41] M. I. Aroyo, J. M. Perez-Mato, C. Capillas, E. Kroumova, S. Ivantchev, G. Madariaga, A. Kirov, H. Wondratschek, *Z. Kristallogr.* **2006**, *221*, 15–27, https://doi.org/10.1524/zkri.2006.221.1.15.

[42] M. I. Aroyo, A. Kirov, C. Capillas, J. M. Perez-Mato, H. Wondratschek, *Acta Cryst. A* **2006**, *62*, 115–128, https://doi.org/10.1107/S0108767305040286.

[43] M. I. Aroyo, J. M. Perez-Mato, D. Orobengoa, E. Tasci, G. De La Flor, A. Kirov, *Bulg. Chem. Commun.* **2011**, *43*, 183–197.

[44] A. Otero-de-la-Roza, E. R. Johnson, V. Luaña, *Comput. Phys. Commun.* **2014**, *185*, 1007–1018, https://doi.org/10.1016/j.cpc.2013.10.026.

[45] A. Otero-de-la-Roza, M. A. Blanco, A. M. Pendás, V. Luaña, *Comput. Phys. Commun.* **2009**, *180*, 157–166, https://doi.org/10.1016/j.cpc.2008.07.018.

[46] B. Winkler, J. Zemann, V. Milman, *Acta Cryst. B* **2000**, *56*, 648–653, https://doi.org/10.1107/S0108768100003621.

[47] R. J. Reeder, *Carbonates: Mineralogy and Chemistry*, Mineralogical Society of America, Washington, D.C. **1983**.

[48] B. D. Botan-Neto, D. Santamaría-Pérez, *CrystEngComm* **2025**, *27*, 6865–6883, https://doi.org/10.1039/D5CE00682A.

[49] M. Isshiki, T. Irifune, K. Hirose, S. Ono, Y. Ohishi, T. Watanuki, E. Nishibori, M. Takata, M. Sakata, *Nature* **2004**, *427*, 60–63, https://doi.org/10.1038/nature02181.

[50] S. Arapan, R. Ahuja, *Phys. Rev. B Condens Matter. Mater. Phys.* **2010**, *82*, 184115, https://doi.org/10.1103/PhysRevB.82.184115.

[51] X. Yuan, X. Xiong, G. Zhang, R. A. Mayanovic, *J. Raman Spectrosc.* **2020**, *51*, 1248–1259, https://doi.org/10.1002/jrs.5893.

[52] T. Boehm, D. Mehta, *Ber. Dtsch. Chem. Ges.* **1938**, *71*, 1797–1802, https://doi.org/10.1002/cber.19380710904.

[53] D. Corradini, F.-X. Coudert, R. Vuilleumier, *Nat. Chem.* **2016**, *8*, 454–460, https://doi.org/10.1038/nchem.2450.

[54] D. N. Sagatova, N. E. Sagatov, P. N. Gavryushkin, *Inorg. Chem. Commun.* **2024**, *167*, 112808, https://doi.org/10.1016/j.inoche.2024.112808.

[55] D. Spahr, J. König, L. Bayarjargal, V. Milman, A. Perlov, H.-P. Liermann, B. Winkler, *J. Am. Chem. Soc.* **2022**, *144*, 2899–2904, https://doi.org/10.1021/jacs.2c00351.

[56] D. Spahr, L. Bayarjargal, M. Bykov, L. Brüning, P. L. Jurzick, V. Milman, N. Giordano, M. Mezouar, B. Winkler, *Angew. Chem. Int. Ed.* **2024**, *63*, e202409822.

[57] D. Spahr, L. Bayarjargal, M. Bykov, L. Brüning, P. L. Jurzick, Y. Wang, V. Milman, K. Refson, M. Mezouar, B. Winkler, *Commun. Chem.* **2024**, *7*, 238, https://doi.org/10.1038/s42004-024-01293-1.

[58] D. Spahr, L. Bayarjargal, M. Bykov, L. Brüning, T. H. Reuter, V. Milman, H.-P. Liermann, B. Winkler, *Dalton Trans.* **2024**, *53*, 40–44, https://doi.org/10.1039/D3DT03673A.

[59] D. Spahr, L. Bayarjargal, E. Haussühl, R. Luchitskaia, A. Friedrich, V. Milman, T. Fedotenko, B. Winkler, *Chem. Commun.* **2023**, *59*, 11951–11954, https://doi.org/10.1039/D3CC03324D.

[60] V. Cerantola, E. Bykova, I. Kupenko, M. Merlini, L. Ismailova, C. McCammon, M. Bykov, A. I. Chumakov, S. Petitgirard, I. Kantor, V. Svitlyk, J. Jacobs, M. Hanfland, M. Mezouar, C. Prescher, R. Rüffer, V. B. Prakapenka, L. Dubrovinsky, *Nat. Commun.* **2017**, *8*, 15960, https://doi.org/10.1038/ncomms15960.

[61] E. Boulard, D. Pan, G. Galli, Z. Liu, W. L. Mao, *Nat. Commun.* **2015**, *6*, 6311, https://doi.org/10.1038/ncomms7311.

[62] E. Boulard, A. Gloter, A. Corgne, D. Antonangeli, A.-L. Auzende, J.-P. Perrillat, F. Guyot, G. Fiquet, *Proc. Natl. Acad. Sci. USA* **2011**, *108*, 5184–5187, https://doi.org/10.1073/pnas.1016934108.

[63] D. Laniel, J. Binck, B. Winkler, S. Vogel, T. Fedotenko, S. Chariton, V. Prakapenka, V. Milman, W. Schnick, L. Dubrovinsky, N. Dubrovinskaia, *Acta Cryst. B* **2021**, *77*, 131–137, https://doi.org/10.1107/S2052520620016650.

[64] J. König, D. Spahr, L. Bayarjargal, P. N. Gavryushkin, D. Sagatova, N. Sagatov, V. Milman, H.-P. Liermann, B. Winkler, *ACS Earth Space Chem.* **2022**, *6*, 73–80.

[65] V. Cerantola, C. J. Sahle, S. Petitgirard, M. Wu, S. Checchia, C. Weis, M. Di Michiel, G. B. M. Vaughan, I. E. Collings, R. Arató, M. Wilke, A. P. Jones, M. Hanfland, J. S. Tse, *Commun. Earth Environ.* **2023**, *4*, 67, https://doi.org/10.1038/s43247-023-00722-8.

[66] X. Yao, C. Xie, X. Dong, A. R. Oganov, Q. Zeng, *Phys. Rev. B* **2018**, *98*, 014108, https://doi.org/10.1103/PhysRevB.98.014108.

[67] D. Spahr, J. König, L. Bayarjargal, P. N. Gavryushkin, V. Milman, H.-P. Liermann, B. Winkler, *Inorg. Chem.* **2021**, *60*, 14504–14508, https://doi.org/10.1021/acs.inorgchem.1c01900.

[68] J. Binck, D. Laniel, L. Bayarjargal, S. Khandarkhaeva, T. Fedotenko, A. Aslandukov, K. Glazyrin, V. Milman, S. Chariton, V. B. Prakapenka, N. Dubrovinskaia, L. Dubrovinsky, B. Winkler, *Am. Mineral.* **2022**, *107*, 336–342, https://doi.org/10.2138/am-2021-7872.

[69] P. N. Gavryushkin, D. N. Sagatova, N. Sagatov, K. D. Litasov, *ACS Earth Space Chem.* **2021**, *5*, 1948–1957, https://doi.org/10.1021/acsearthspacechem.1c00084.

[70] A. Pantousas, G. Aprilis, A. Aslandukova, I. Kupenko, X. Li, W. Zhou, P. Leveque, M. Hanfland, L. Dubrovinsky, A. Pakhomova, **2025**, https://doi.org/10.21203/rs.3.rs-7516922/v1.

[71] Y. Wang, L. Bayarjargal, E. Bykova, D. Spahr, M. Bykov, V. Milman, N. Giordano, T. Fedotenko, H. P. Liermann, B. Winkler, *Cryst. Growth Des.* **2024**, *24*, 4143–4150, https://doi.org/10.1021/acs.cgd.4c00225.

[72] V. Kovalev, D. Spahr, B. Winkler, L. Bayarjargal, L. Wedek, A. Aslandukova, A. Pakhomova, G. Garbarino, E. Bykova, *Commun. Chem.* **2025**, *8*, 66, https://doi.org/10.1038/s42004-025-01450-0.

[73] D. Santamaría-Pérez, A. Vegas, F. Liebau in *Semiconductor Nanocrystals and Silicate Nanoparticles*, Springer-Verlag, Berlin/Heidelberg, **2005**, pp. 121–177, https://doi.org/10.1007/b11020.

[74] D. Scelta, M. Ceppatelli, R. Ballerini, A. Hajeb, M. Peruzzini, R. Bini, *Rev. Sci. Instrum.* **2018**, *89*, 053903. https://doi.org/10.1063/1.5011286.

[75] I. F. Silvera, A. D. Chijioke, W. J. Nellis, A. Soldatov, J. Tempere, *Phys. Status Solidi B* **2007**, *244*, 460–467.

[76] D. Santamaría-Pérez, R. Chuliá-Jordán, B. D. Botan-Neto, G. Bera, J. Pellicer-Porres, L. Bayarjargal, A. Otero-de-la-Roza, C. Popescu, *Phys. Chem. Chem. Phys.* **2025**, *27*, 3320–3329, https://doi.org/10.1039/D4CP04200J.

[77] H.-P. Liermann, Z. Konôpková, W. Morgenroth, K. Glazyrin, J. Bednarčik, E. E. McBride, S. Petitgirard, J. T. Delitz, M. Wendt, Y. Bican, A. Ehnes, I. Schwark, A. Rothkirch, M. Tischer, J. Heuer, H. Schulte-Schrepping, T. Kracht, H. Franz, *J. Synchrotron Radiat.* **2015**, *22*, 908–924, https://doi.org/10.1107/S1600577515005937.

[78] C. Prescher, V. B. Prakapenka, *High Press Res.* **2015**, *35*, 223–230.

[79] Rigaku Oxford Diffraction, CrysAlisPro, version 171.44.122a; Rigaku Oxford Diffraction Ltd.: Yarnton, England, **2025**.

[80] A. Aslandukov, M. Aslandukov, N. Dubrovinskaia, L. Dubrovinsky, *J. Appl. Crystallogr.* **2022**, *55*, 1383–1391, https://doi.org/10.1107/S1600576722008081.

[81] O. V. Dolomanov, L. J. Bourhis, R. J. Gildea, J. A. K. Howard, H. Puschmann, *J. Appl. Crystallogr.* **2009**, *42*, 339–341, https://doi.org/10.1107/S0021889808042726.

[82] G. M. Sheldrick, *Acta Cryst. A* **2015**, *71*, 3–8, https://doi.org/10.1107/S2053273314026370.

[83] G. M. Sheldrick, *Acta Cryst. C* **2015**, *71*, 3–8, https://doi.org/10.1107/S2053229614024218.

[84] P. E. Blöchl, *Phys. Rev. B* **1994**, *50*, 17953–17979.

[85] P. Giannozzi, O. Andreussi, T. Brumme, O. Bunau, M. Buongiorno Nardelli, M. Calandra, R. Car, C. Cavazzoni, D. Ceresoli, M. Cococcioni, N. Colonna, I. Carnimeo, A. Dal Corso, S. de Gironcoli, P. Delugas, R. A. DiStasio, A. Ferretti, A. Floris, G. Fratesi, G. Fugallo, R. Gebauer, U. Gerstmann, F. Giustino, T. Gorni, J. Jia, M. Kawamura, H.-Y. Ko, A. Kokalj, E. Küçükbenli, M. Lazzeri, et al. *J. Phys.: Condens. Matter* **2017**, *29*, 465901.

[86] J. P. Perdew, K. Burke, M. Ernzerhof, *Phys. Rev. Lett.* **1996**, *77*, 3865–3868, https://doi.org/10.1103/PhysRevLett.77.3865.

[87] A. D. Becke, *J. Chem. Phys.* **1986**, *85*, 7184–7187, https://doi.org/10.1063/1.451353.

[88] A. D. Becke, E. R. Johnson, *J. Chem. Phys.* **2007**, *127*, 154108, https://doi.org/10.1063/1.2795701.

[89] A. Otero-de-la-Roza, E. R. Johnson, *J. Chem. Phys.* **2012**, *136*, 174109, https://doi.org/10.1063/1.4705760.

[90] A. Dal Corso, *Comput. Mater. Sci.* **2014**, *95*, 337–350, https://doi.org/10.1016/j.commatsci.2014.07.043.

[91] A. Otero-de-la-Roza, V. Luaña, *Comput. Phys. Commun.* **2011**, *182*, 1708–1720, https://doi.org/10.1016/j.cpc.2011.04.016.

[92] A. Otero-de-la-Roza, D. Abbasi-Pérez, V. Luaña, *Comput. Phys. Commun.* **2011**, *182*, 2232–2248, https://doi.org/10.1016/j.cpc.2011.05.009.

[93] R. Dovesi, A. Erba, R. Orlando, C. M. Zicovich-Wilson, B. Civalleri, L. Maschio, M. Rérat, S. Casassa, J. Baima, S. Salustro, B. Kirtman, *WIREs Comput. Mol. Sci.* **2018**, *8*, e1360, https://doi.org/10.1002/wcms.1360.

[94] D. Vilela Oliveira, J. Laun, M. F. Peintinger, T. Bredow, *J. Comput. Chem.* **2019**, *40*, 2364–2376, https://doi.org/10.1002/jcc.26013.

[95] A. D. Becke, *J. Chem. Phys.* **1993**, *98*, 5648–5652, https://doi.org/10.1063/1.464913.

[96] C. Lee, W. Yang, R. G. Parr, *Phys. Rev. B* **1988**, *37*, 785–789, https://doi.org/10.1103/PhysRevB.37.785.

[97] L. Maschio, B. Kirtman, M. Rérat, R. Orlando, R. Dovesi, *J. Chem. Phys.* **2013**, *139*, 164102, https://doi.org/10.1063/1.4824443.

[98] L. Maschio, B. Kirtman, M. Rérat, R. Orlando, R. Dovesi, *J. Chem. Phys.* **2013**, *139*, 164102, https://doi.org/10.1063/1.4824443.
[99] P. Hohenberg, W. Kohn, *Phys. Rev.* **1964**, *136*, B864–B871, https://doi.org/10.1103/PhysRev.136.B864.
[100] S. J. Clark, M. D. Segall, C. J. Pickard, P. J. Hasnip, M. I. J. Probert, K. Refson, M. C. Payne, *Z Kristallogr Cryst Mater* **2005**, *220*, 567–570, https://doi.org/10.1524/zkri.220.5.567.65075.
[101] K. Lejaeghere, G. Bihlmayer, T. Björkman, P. Blaha, S. Blügel, V. Blum, D. Caliste, I. E. Castelli, S. J. Clark, A. Dal Corso, S. de Gironcoli, T. Deutsch, J. K. Dewhurst, I. Di Marco, C. Draxl, M. Dułak, O. Eriksson, J. A. Flores-Livas, K. F. Garrity, L. Genovese, P. Giannozzi, M. Giantomassi, S. Goedecker, X. Gonze, O. Grånäs, E. K. U. Gross, A. Gulans, F. Gygi, D. R. Hamann, P. J. Hasnip, et al. *Science (1979)* **2016**, *351*, aad3000.
[102] H. J. Monkhorst, J. D. Pack, *Phys. Rev. B* **1976**, *13*, 5188–5192, https://doi.org/10.1103/PhysRevB.13.5188.
[103] S. Baroni, S. de Gironcoli, A. Dal Corso, P. Giannozzi, *Rev. Mod. Phys.* **2001**, *73*, 515–562, https://doi.org/10.1103/RevModPhys.73.515.
[104] K. Refson, P. R. Tulip, S. J. Clark, *Phys. Rev. B* **2006**, *73*, 155114, https://doi.org/10.1103/PhysRevB.73.155114.
[105] K. Miwa, *Phys. Rev. B* **2011**, *84*, 094304, https://doi.org/10.1103/PhysRevB.84.094304.
[106] D. Spahr, L. Bayarjargal, L. Brüning, V. Kovalev, E. Bykova, M. Bykov, V. Milman, M. Mezouar, B. Winkler, *JACS Au* **2025**, *5*, 4675–4680.
[107] A. Togo, I. Tanaka, *Scr. Mater.* **2015**, *108*, 1–5, https://doi.org/10.1016/j.scriptamat.2015.07.021.
[108] L. Liu, *Nature* **1983**, *303*, 508–509, https://doi.org/10.1038/303508a0.
[109] V. Iota, C.-S. Yoo, J.-H. Klepeis, Z. Jenei, W. Evans, H. Cynn, *Nat. Mater.* **2007**, *6*, 34–38, https://doi.org/10.1038/nmat1800.
[110] J. Li, O. Sode, G. A. Voth, S. Hirata, *Nat. Commun.* **2013**, *4*, 2647, https://doi.org/10.1038/ncomms3647.
[111] P. Richet, H. Mao, P. M. Bell, *J. Geophys. Res. Solid Earth* **1988**, *93*, 15279–15288, https://doi.org/10.1029/JB093iB12p15279.
[112] V. Swamy, S. K. Saxena, B. Sundman, J. Zhang, *J Geophys. Res. Solid Earth* **1994**, *99*, 11787–11794, https://doi.org/10.1029/93JB02968.
[113] M. Akaogi, A. Navrotsky, *Phys. Earth Planet Int.* **1984**, *36*, 124–134, https://doi.org/10.1016/0031-9201(84)90013-X.
[114] D. Andrault, G. Fiquet, F. Guyot, M. Hanfland, *Science* **1998**, *282*, 720–724, https://doi.org/10.1126/science.282.5389.720.
[115] L. Merrill, W. A. Bassett, *Acta Cryst. B* **1975**, *31*, 343–349, https://doi.org/10.1107/S0567740875002774.
[116] P. N. Gavryushkin, N. S. Martirosyan, T. M. Inerbaev, Z. I. Popov, S. V. Rashchenko, A. Y. Likhacheva, S. S. Lobanov, A. F. Goncharov, V. B. Prakapenka, K. D. Litasov, *Cryst. Growth Des.* **2017**, *17*, 6291–6296.
[117] D. Smith, K. V. Lawler, M. Martinez-Canales, A. W. Daykin, Z. Fussell, G. A. Smith, C. Childs, J. S. Smith, C. J. Pickard, A. Salamat, *Phys. Rev. Mater.* **2018**, *2*, 013605, https://doi.org/10.1103/PhysRevMaterials.2.013605.
[118] C. Capillas, E. S. Tasci, G. de la Flor, D. Orobengoa, J. M. Perez-Mato, M. I. Aroyo, *Zeitschrift für Kristallographie* **2011**, *226*, 186–196, https://doi.org/10.1524/zkri.2011.1321.
[119] L. Bayarjargal, C.-J. Fruhner, N. Schrodt, B. Winkler, *Phys. Earth Planet Int.* **2018**, *281*, 31–45, https://doi.org/10.1016/j.pepi.2018.05.002.
[120] E. J. Blancas, Á. Lobato, F. Izquierdo-Ruiz, A. M. Márquez, J. M. Recio, P. Nath, J. J. Plata, A. Otero-de-la-Roza, *NPJ Comput. Mater.* **2024**, *10*, 267.
[121] Deposition Numbers 2494285 ($Ca_2Si(CO_3)_4$ at 39.5 GPa), 2494286 ($Ca_2Si(CO_3)_4$ at ambient pressure), and 2494194 ($Ca_2C_4O_{10}$ at 39.5 GPa) contain the supplementary crystallographic data for this paper. These data are available free of charge from the joint Cambridge Crystallographic Data Centre (CCDC) and Fachinformationszentrum Karlsruhe (FIZ) Access Structures service.

Manuscript received: November 12, 2025
Revised manuscript received: January 05, 2026
Manuscript accepted: January 15, 2026
Version of record online: January 22, 2026